AIMS Mathematics, 9(11): 32757–32781.
DOI:10.3934/math.20241567
Received: 23 September 2024
Revised: 29 October 2024
Accepted: 14 November 2024
Published: 19 November 2024

http://www.aimspress.com/journal/Math

Research article

Optimal homotopy analysis method for (2+1) time-fractional nonlinear biological population model using J-transform

Khalid K. Ali[1,*], **Mohamed S. Mohamed**[2] **and M. Maneea**[3]

[1] Mathematics Department, Faculty of Science, Al-Azhar University, Nasr-City, Cairo, Egypt
[2] Department of Mathematics, College of Science, Taif University, P.O. Box 11099, Taif 21944, Saudi Arabia
[3] Faculty of Engineering, MTI University, Cairo, Egypt

* **Correspondence:** Email: khalidkaram2012@azhar.edu.eg; Tel: +201033530861.

Abstract: This paper presents a comprehensive study of the (2+1) time-fractional nonlinear generalized biological population model (TFNBPM) using the J-transform combined with the optimal homotopy analysis method, a robust semi-analytical technique. The primary focus is to derive analytical solutions for the model and provide a thorough investigation of the convergence properties of these solutions. The proposed method allows for flexibility and accuracy in handling nonlinear fractional differential equations (NFDEs), demonstrating its efficacy through a series of detailed analyses. To validate the results, we present a set of 2D and 3D graphical representations of the solutions, illustrating the dynamic behavior of the biological population over time and space. These visualizations provide insightful perspectives on the population dynamics governed by the model. Additionally, a comparative study is conducted, where our results are juxtaposed with those obtained using other established techniques from the literature. The comparisons underscore the advantages of optimal homotopy analysis J-transform method (optimal HAJ-TM), highlighting its consistency and superior convergence in solving complex fractional models.

Keywords: fractional derivatives; J-transform, optimal homotopy analysis method; biological population model
Mathematics Subject Classification: 35A25, 35C10, 35E15

1. Introduction

Biological population models are crucial tools in understanding the dynamics of species populations over time. These models incorporate various factors that affect the population and interactions between these factors; this allows researchers to identify key drivers of population change and assess the impact

of environmental changes, and develop effective conservation strategies. Furthermore, population models can be used to predict the long-term viability of species and inform decisions about habitat preservation, species reintroduction, and invasive species management. The complexity of biological systems often necessitates the use of nonlinear differential equations to accurately represent these interactions [1–3]. Recently, the incorporation of fractional calculus into these models has gained attention, as it allows for a more nuanced depiction of memory and hereditary properties inherent in biological systems. The time-fractional derivatives provide a flexible framework that can capture the long-term dependencies and anomalous diffusion processes observed in ecological contexts. As a result, time-fractional models have proven to be more effective in describing real-world biological phenomena compared to traditional integer-order models [4, 5]. This mathematical field has received considerable attention because of its capability to model processes that exhibit anomalous behavior and memory effects, which are not adequately captured by integer-order models. Fractional differential equations (FDEs) are particularly useful in describing systems with long-range temporal or spatial dependencies, making them applicable in various disciplines such as physics [6], engineering [7, 8], biology [9, 10], and even natural phenomena [11]. The versatility of FDEs lies in their ability to incorporate history-dependent effects, providing a more accurate and comprehensive framework for modeling complex dynamical systems.

Solving FDEs present unique challenges due to their non-local properties and the complexity of fractional derivatives. Various methods have been developed to address these challenges, broadly categorized into numerical, analytical, and semi-analytical approaches. Numerical methods, such as finite difference and finite element methods, discretize the equations to approximate solutions, offering flexibility and robustness in handling complex boundary conditions and geometries. However, they often require significant computational resources and can be less insightful regarding the underlying dynamics [12, 13]. Analytical methods aim to provide exact solutions, or exact solutions under conditions offering deep insights into the behavior of the system, such as invariant subspace, local symmetry, and Lie symmetry analysis [14–16]. Techniques such as the Laplace transform and Mittag-Leffler functions are often employed, though finding closed-form solutions can be difficult or impossible for highly nonlinear problems [17, 18]. Semi-analytical methods, such as the homotopy analysis method (HAM) and the Adomian decomposition method, bridge the gap between numerical and analytical techniques. These methods provide approximate solutions that converge to the exact solution, combining the interpretative power of analytical methods with the practical applicability of numerical approaches [19, 20].

Maitama and Zhao, in 2020 [21], introduced a new transform called the J-transform, which is an adaptation of the widely recognized Sumudu transform and the Natural transform. Additionally, they established the connection between the J-transform and the other integral transforms. In 2022, Singh et al. [22], applied the J transform with the HAM and variation iteration method to solve the telegraph equation. Recently, Singh et al. [23], also applied the J-transform to the differential transform to solve a hyperbolic wave equation. So far, the use of the J-transform in solving differential equations remains limited despite its efficiency and accurate results.

The TFNBPM has been examined both analytically and numerically by various researchers, providing a deeper understanding of the underlying mechanisms and behaviors. Among them, Srivastava et al. [24], provided an analytical solution for the TFNBPM using the fractional reduced differential transform method by employing the Caputo fractional derivative. Acan et al. [25], presented

exact solutions for the TFNBPM using reduced differential transform with conformable fractional derivative. Veeresha and Prakasha [26], presented the solution of the TFNBPM using the natural decomposition method. Ziane et al. [27], solved the TFNBPM using HAM utilizing local fractional derivatives. Alaroud et al. [28], provided an efficient solution using the Laplace residual power series method.

The objective of this article is to explore the optimal HAM with J-transform to present solutions for the TFNBPM using Caputo fractional derivative (CFD). By leveraging this technique, our goal is to offer a thorough understanding of the model's dynamics and offer robust solutions that can be used to analyze complex biological systems.

This article is structured as follows: In Section 2, we introduce several notations about the CFD and the J-transform with their most important relations. A detailed analysis of the model being examined is outlined in Section 3. Section 4 offers an overview of the analytical method used with its convergence analysis. In Section 5, we introduce the steps of the analytical solutions for this particular model using different initial conditions. In the sixth section, we display various figures illustrating the obtained solutions at different parameters. Finally, the conclusion section summarizes our findings and highlights the key outcomes of this research.

2. Basic notations

In this part, we present the fundamentals of CFD and the J-transform with its basic properties.

2.1. Fundamentals of Caputo fractional derivatives

The Grunwald-Letnikov, Weyl, Riemann-Liouville, Marchaud, Caputo, and Riesz definitions of fractional derivatives strive to retain the typical characteristics of the normal derivative. Among these definitions, the only universally shared property is linearity. Some specific properties associated with each definition were listed in [29–31].

Most researchers in fractional calculus focus on investigating the CFD, which has gained popularity for simulating real-world problems due to two primary reasons. Firstly, the CFD is bounded because the derivative of a constant yields zero, and secondly, it allows for expressing initial conditions through an integer-order derivative. It is important to emphasize that Caputo's definition applies exclusively to functions that exhibit differentiability.

Definition 2.1. *[29] The CFD of θ order is defined by*

$$ {}^{C}\mathsf{D}_{U}^{\theta} f(U) = \begin{cases} \mathfrak{J}^{\mathsf{k}-\theta} \dfrac{\mathsf{d}^{\mathsf{k}}}{\mathsf{d}U^{\mathsf{k}}} f(U), & \mathsf{k}-1 < \theta < \mathsf{k}, \\ \dfrac{\mathsf{d}^{\mathsf{k}}}{\mathsf{d}U^{\mathsf{n}}} f(U), & \theta = \mathsf{k}, \end{cases} \tag{2.1} $$

where $\mathfrak{J}^{\mathsf{k}-\theta}$ represents the Riemann-Liouville (RL) fractional integral, which can be described as

$$ \mathfrak{J}^{\theta} f(U) = \frac{1}{\Gamma(\theta)} \int_{0}^{U} (U-\Upsilon)^{\theta-1} f(\Upsilon)\, d\Upsilon, \quad U > 0, \ \theta \in R^{+}, \tag{2.2} $$

where, R^{+} denotes all real positive numbers, and the function $\Gamma(.)$ represents the well-known Gamma function. The operator $\mathfrak{J}^{\theta}$ exhibits the following characteristics for $f(U) \in$ space C_{μ}, $\mu \in R$, and

$\mu \geq -1$, $\alpha, \beta \geq 0$ *and* $\upsilon \geq -1$*:*

$$\mathfrak{J}^{\alpha}\mathfrak{J}^{\beta}f(U) = \mathfrak{J}^{\alpha+\beta}f(U). \tag{2.3}$$

$$\mathfrak{J}^{\alpha}\mathfrak{J}^{\beta}f(U) = \mathfrak{J}^{\beta}\mathfrak{J}^{\alpha}f(U). \tag{2.4}$$

$$\mathfrak{J}^{\alpha}U^{\upsilon} = \frac{\Gamma(\upsilon+1)}{\Gamma(\upsilon+1+\alpha)}U^{\upsilon+\alpha}. \tag{2.5}$$

CFD satisfies the following properties:

$$^{C}\mathsf{D}_{U}^{\theta}\Big[\mathfrak{J}^{\theta}f(U)\Big] = f(U). \tag{2.6}$$

$$\mathfrak{J}^{\theta}\Big[\,^{C}\mathsf{D}_{U}^{\theta}f(U)\Big] = f(U) - \sum_{\iota=0}^{\mathsf{k}-1} f^{\iota}(0)\frac{U^{\iota}}{\iota!}, \quad U > 0. \tag{2.7}$$

$$^{C}\mathsf{D}_{U}^{\theta}U^{\nu} = \frac{\Gamma(\nu+1)}{\Gamma(\nu+1-\theta)}U^{\nu-\theta}. \tag{2.8}$$

2.2. An overview of the J-transform

The J-transform (JT) as presented in [21] is

Definition 2.2. *The JT of a function* $\mathcal{W}(t) \in \Omega$ *is defined as*

$$J[\mathcal{W}(t)](\mathsf{s},\mathsf{v}) = \mathcal{W}(t)(\mathsf{s},\mathsf{v}) = \mathsf{v}\int_{0}^{\infty} exp\Big(-\frac{\mathsf{s}t}{\mathsf{v}}\Big)\mathcal{W}(t)\mathsf{d}t, \tag{2.9}$$

where s *and* v *are the variables of transformation, and* Ω *are the functions of exponential order:* $\Omega = \Big\{\mathcal{W}(t) : \exists\, \mathsf{r}_1, \mathsf{r}_2 > 0, 0 < \mathcal{E} < \infty\Big\}$*, such that:*

$$|\mathcal{W}(t)| \leq \mathcal{E}\, exp\Big(\frac{|t|}{\mathsf{r}_i}\Big), \; for \quad t \in (-1)^{i} \times [0,\infty).$$

The definition is valid under the condition that, the integral exists.

These are some of the important properties of the JT that we use in the research.

Lemma 2.1. *[22]*
(a) If the two functions $\mathsf{g}(t)$ *and* $\mathsf{h}(t)$ *are* $\in \Omega$ *have the JT* $\mathcal{G}(\mathsf{s},\mathsf{v})$ *and* $\mathcal{H}(\mathsf{s},\mathsf{v})$*, respectively, then,*
(i). (Linearity of JT)

$$J[\mathcal{K}_1\,\mathsf{g}(\mathsf{x},t) + \mathcal{K}_2\,\mathsf{h}(\mathsf{x},t)](\mathsf{s},\mathsf{v}) = \mathcal{K}_1\,\mathcal{G}(\mathsf{x},\mathsf{s},\mathsf{v}) + \mathcal{K}_2\,\mathcal{H}(\mathsf{x},\mathsf{s},\mathsf{v}).$$

(ii). (Convolution of JT)

$$J[\mathsf{g} * \mathsf{h}](\mathsf{s},\mathsf{v}) = \frac{1}{\mathsf{v}}\mathcal{G}(\mathsf{s},\mathsf{v})\,\mathcal{H}(\mathsf{s},\mathsf{v}).$$

(b) For power functions,

$$J\Big[\frac{t^{\ell\theta+\mathsf{b}}}{\Gamma(\ell\theta+\mathsf{b}+1)}\Big](\mathsf{s},\mathsf{v}) = \frac{\mathsf{v}^{\ell\theta+\mathsf{b}+2}}{\mathsf{s}^{\ell\theta+\mathsf{b}+1}}, \quad for\ \ell, \mathsf{b} = 0,1,2,...,$$

where $\Gamma(.)$ *represents the well-known Gamma function.*
(c) If the function $\mathsf{p}(\mathsf{x},t) \in \Omega$ *has the JT* $\mathcal{P}(\mathsf{s},\mathsf{v})$*, then the JT of* $\frac{\partial^{\mathsf{j}} p(\mathsf{x},t)}{\partial t^{\mathsf{j}}} \in \Omega$ *is*

$$J\left[\frac{\partial^{\mathsf{j}} p(\mathsf{x},t)}{\partial t^{\mathsf{j}}}\right](\mathsf{s},\mathsf{v}) = \frac{\mathsf{s}^{\mathsf{j}}}{\mathsf{v}^{\mathsf{j}}}\mathcal{P}(\mathsf{x},\mathsf{s},\mathsf{v}) - \sum_{\iota=1}^{\mathsf{j}} \frac{\mathsf{s}^{\mathsf{j}-\iota}}{\mathsf{v}^{\mathsf{j}-(\iota+1)}} \frac{\partial^{\iota-1}\mathsf{p}(\mathsf{x},0^{+})}{\partial t^{\iota-1}}, \quad \mathsf{j} \geq 1.$$

(d) If the CFD of θ *order is* ${}^{C}\mathsf{D}_{t}^{\theta} f(\mathsf{x},t)$*, then,*

$$J\left[{}^{C}\mathsf{D}_{t}^{\theta} f(\mathsf{x},t)\right](\mathsf{s},\mathsf{v}) = \frac{\mathsf{s}^{\theta}}{\mathsf{v}^{\theta}}\mathcal{F}(\mathsf{x},\mathsf{s},\mathsf{v}) - \sum_{\iota=1}^{m} \frac{\mathsf{s}^{\theta-\iota}}{\mathsf{v}^{\theta-(\iota+1)}} \frac{\partial^{\iota-1} f(\mathsf{x},0^{+})}{\partial t^{\iota-1}}, \quad m-1 < \theta \leq m.$$

3. Theoretical framework of the TFNBPM

The general form of the TFNBPM in two dimensions is

$${}^{C}\mathsf{D}_{\mathbf{t}}^{\mathcal{B}} \mathcal{Z}(\mathsf{x},y,\mathbf{t}) = \frac{\partial^2 \mathcal{Z}^2}{\partial \mathsf{x}^2} + \frac{\partial^2 \mathcal{Z}^2}{\partial y^2} + \rho(\mathcal{Z}), \tag{3.1}$$

under initial condition

$$\mathcal{Z}_0(\mathsf{x},y,\mathbf{t}) = \mathcal{Z}(\mathsf{x},y,0).$$

Where $\mathcal{Z} = \mathcal{Z}(\mathsf{x},y,\mathbf{t})$ is the population density or the state variable of interest, which depends on the spatial coordinates x, and y as well as the time $\mathbf{t}$, the spatial variables or coordinates over which the population density $\mathcal{Z}$ is distributed, and $\mathbf{t}$ is the time over which the population evolves, ρ signifies the growth rate or interaction of the population, incorporating factors like birth, death, competition, and other ecological interactions, and $\mathcal{B}$ is the order of CFD ($0 < \mathcal{B} \leq 1$).

$\rho(\mathcal{Z})$ can take different forms, each with its own significance:
(*i*). $\rho(\mathcal{Z}) = C\mathcal{Z}$, where C is a constant. This is called the Malthusian law for the generalized biological population model; this is attributed to Thomas Malthus (1798), who shared his perspective on how population growth impacts the food supply. His theory is based on two fundamental principles:
- Population increases in geometric rate (1, 2, 4, 16, 32, ...).
- Food production rises at an arithmetic rate (1, 2, 3, 4,...).
(*ii*). $\rho(\mathcal{Z}) = C_1\mathcal{Z} + C_2\mathcal{Z}^2$, where C_1 and C_2 are constants. This is called Verhulst law; this corresponds to Pierre-François Verhulst. It is a mathematical model used to describe the growth or decay of a biological population interacting with its environment. It is a generalization of the logistic equation and is often used to model population dynamics in ecology and biology.

From Figure 1, one can notice that, when the population grows exponentially (geometrically), the food production increases linearly (arithmetically), and eventually the demand for food will outstrip supply. The point that indicates the Malthusian trap, some-times called a Malthusian catastrophe, refers to a situation where population growth surpasses agricultural production, leading to a crisis. This point indicates a critical threshold where the available resources, particularly food, are insufficient to sustain the population.

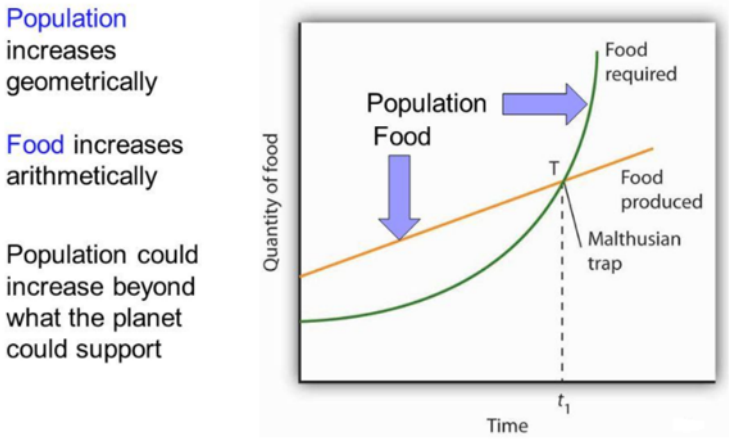

Figure 1. Population growth according to Malthusian law.

Figure 2 clarifies Verhulst's Law for the biological population model, it also known as the logistic growth model; it describes how biological populations grow in a constrained environment. Unlike exponential growth, which assumes unlimited resources and results in a population increasing at a constant rate, Verhulst's model incorporates the concept of carrying capacity. This means that as the population size approaches the environment's limit, growth slows and eventually stabilizes. The logistic growth model is represented by an S-shaped curve, where the population initially grows exponentially but then tapers off as it encounters resource limitations, leading to a stable equilibrium.

In this study, we deal with the two laws at different initial conditions.

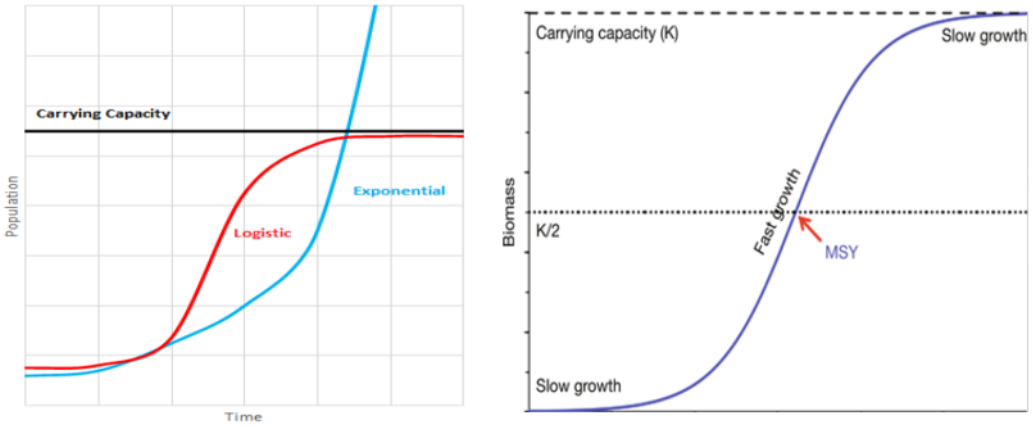

Figure 2. Population growth according to Verhulst law.

4. Analysis of the optimal HA*J*-TM

The HAM was first introduced by Liao Shijun in 1992; then this method underwent to some modifications by Liao and others [32]. Marinca and Herisanu [33], produced a significant modification to optimize the convergence of solutions to nonlinear problems and present the optimal homotopy asymptotic method for the first time. In 2010, Liao presented other modifications [34] for the method and called it the optimal homotopy analysis method. Since then, it has become a valuable tool

in applied mathematics and engineering, facilitating the analysis and solution of various nonlinear systems across multiple disciplines.

In this part, we explore the steps for finding an approximate solution for the TFNBPM using optimal HAM and JT instead of using Laplace transform. These steps are outlined as follows:

First, the model Eq (3.1) can be expressed as

$$\mathscr{N}\{{}^{C}\mathsf{D}_{\mathsf{t}}^{\mathcal{B}}\mathcal{Z}(\mathsf{x},y,\mathbf{t})\}=0,\quad 0<\mathcal{B}\leq 1, \tag{4.1}$$

then, impose JT on the examined model (3.1), we obtain

$$J[\mathcal{Z}(\mathsf{x},y,\mathbf{t})](\mathsf{s},\mathsf{v})-\frac{\mathsf{v}^2}{\mathsf{s}}\mathcal{Z}_0(\mathsf{x},y,\mathbf{t})+\left(\frac{\mathsf{v}}{\mathsf{s}}\right)^{\mathcal{B}}J\Big[-\frac{\partial^2\mathcal{Z}^2}{\partial\mathsf{x}^2}-\frac{\partial^2\mathcal{Z}^2}{\partial y^2}-\rho(\mathcal{Z})\Big]=0. \tag{4.2}$$

The nonlinear operator, written in the form:

$$\aleph[\varnothing(\mathsf{x},y,\mathbf{t};\wp)]=J[\mathcal{Z}(\mathsf{x},y,\mathbf{t})](\mathsf{s},\mathsf{v})-\frac{\mathsf{v}^2}{\mathsf{s}}\mathcal{Z}_0(\mathsf{x},y,\mathbf{t})+\left(\frac{\mathsf{v}}{\mathsf{s}}\right)^{\mathcal{B}}J\Big[-\frac{\partial^2\mathcal{Z}^2}{\partial\mathsf{x}^2}-\frac{\partial^2\mathcal{Z}^2}{\partial y^2}-\rho(\mathcal{Z})\Big], \tag{4.3}$$

where $\varnothing(\mathsf{x},y,\mathbf{t};\wp)$ is a function that takes real values. The deformation equation of zero-order is written in the following form:

$$(1-\wp)J\{\varnothing(\mathsf{x},y,\mathbf{t};\wp)-\mathcal{Z}_0(\mathsf{x},y,\mathbf{t})\}(\mathsf{s},\mathsf{v})=\wp H(\mathsf{x},y,\mathbf{t})\hbar\aleph[\varnothing(\mathsf{x},y,\mathbf{t};\wp)], \tag{4.4}$$

where $\hbar$ is an auxiliary parameter ($\hbar\neq 0$), $\wp$ called an embedding parameter, $\wp\in[0,1]$, and $H(\mathsf{x},y,\mathbf{t})$ is an auxiliary function.

Clearly, when $\wp=0$, we have $\varnothing(\mathsf{x},y,\mathbf{t};0)=\mathcal{Z}_0(\mathsf{x},y,\mathbf{t})$, and when $\wp=1$, it follows that $\varnothing(\mathsf{x},y,\mathbf{t};1)=\mathcal{Z}(\mathsf{x},y,\mathbf{t})$. As $\wp$ transitions from 0 to 1, the solution transitions from the initial approximation $\mathcal{Z}_0(\mathsf{x},y,\mathbf{t})$ to the final solution $\mathcal{Z}(\mathsf{x},y,\mathbf{t})$. The unknown function $\varnothing$ can be expressed as a Taylor series expansion in terms of $\wp$,

$$\varnothing(\mathsf{x},y,\mathbf{t};\wp)=\mathcal{Z}_0(\mathsf{x},y,\mathbf{t})+\sum_{\iota=1}^{\infty}\mathcal{Z}_\iota(\mathsf{x},y,\mathbf{t})\wp^\iota, \tag{4.5}$$

in which

$$\mathcal{Z}_\iota(\mathsf{x},y,\mathbf{t})=\frac{1}{\iota!}\frac{\partial^\iota\varnothing(\mathsf{x},y,\mathbf{t};\wp)}{\partial\wp^\iota}|_{\wp=0}. \tag{4.6}$$

If $\hbar$ and the auxiliary function H are selected appropriately to ensure that the series in Eq (4.5) converges when $\wp$ is equal to 1, then it can be represented in the form:

$$\mathcal{Z}(\mathsf{x},y,\mathbf{t})=\mathcal{Z}_0(\mathsf{x},y,\mathbf{t})+\sum_{\iota=1}^{\infty}\mathcal{Z}_\iota(\mathsf{x},y,\mathbf{t}). \tag{4.7}$$

Define the vector,

$$\overrightarrow{\mathcal{Z}_\kappa}(\mathsf{x},y,\mathbf{t})=\{\mathcal{Z}_0(\mathsf{x},y,\mathbf{t}),\mathcal{Z}_1(\mathsf{x},y,\mathbf{t}),...,\mathcal{Z}_\kappa(\mathsf{x},y,\mathbf{t})\}. \tag{4.8}$$

The ι-th order deformation equation is derived through the differentiation of Eq (4.4) ι times with respect to $\wp$, then setting $\wp=0$ and dividing by $\iota!$,

$$J\{\mathcal{Z}_\iota(\mathsf{x},y,\mathbf{t})-\chi_\iota\mathcal{Z}_{\iota-1}(\mathsf{x},y,\mathbf{t})\}=\hbar H\mathscr{R}_\iota(\overrightarrow{\mathcal{Z}_{\iota-1}}(\mathsf{x},y,\mathbf{t})), \tag{4.9}$$

where

$$\chi_{\iota} = \begin{cases} 0, & \iota \leq 1, \\ 1, & \iota > 1. \end{cases} \tag{4.10}$$

Setting $H = 1$,

$$\mathcal{Z}_{\iota}(\mathsf{x}, y, \mathbf{t}) = \chi_{\iota}\mathcal{Z}_{\iota-1}(\mathsf{x}, y, \mathbf{t}) + \hbar J^{-1}\{\mathscr{R}_{\iota}(\mathcal{Z}^{\rightarrow}_{\iota-1}(\mathsf{x}, y, \mathbf{t}))\}, \tag{4.11}$$

where

$$\mathscr{R}_{\iota}(\mathcal{Z}^{\rightarrow}_{\iota-1}) = \frac{1}{(\iota-1)!}\frac{\partial^{\iota-1}\mathscr{N}\{\varnothing(\mathsf{x}, y, \mathbf{t}; \wp)\}}{\partial \wp^{\iota-1}}|_{\wp=0}. \tag{4.12}$$

In the optimal HAM, it is known that the value of $\hbar$ governs how the solution converges. Therefore, to determine the region where the solution converges faster, we plot the $\hbar$-curves and observe that the area aligned with the $x-axis$ is where the solution converges quickly. This region usually includes the value -1. More specifically, to determine the optimal value of $\hbar$, we determine the average residual error and minimize it; it is determined by the following formula:

$$\mathcal{E}_{\iota}(\hbar) = \frac{1}{\mathscr{A}\mathscr{B}\mathscr{C}}\sum_{i=0}^{\mathscr{A}}\sum_{j=0}^{\mathscr{B}}\sum_{k=0}^{\mathscr{C}}\Big(\mathscr{N}(\sum_{\mathrm{n}=0}^{\iota}\mathcal{Z}_{\iota}(\frac{i}{\mathscr{A}}, \frac{j}{\mathscr{B}}, \frac{k}{\mathscr{C}}))\Big)^2. \tag{4.13}$$

Equation (4.13) is a nonlinear equation, whose variable function on it is $\hbar$. We solve it to determine the smallest value of $\hbar$ that reduces the average residual error.

4.1. Convergence analysis

Given that the optimal HAJ-TM result in fractional power series, to demonstrate the solution's convergence, consider the following theorems.

Theorem 4.1. *[11, 35] For any series expressed in fractional powers*

$$\sum_{\mathbf{r}=0}^{\infty}\mathsf{C}_{\mathbf{r}}\,\mathbf{t}^{\mathbf{r}\mathcal{B}}, \quad \mathbf{t} \geq 0, \tag{4.14}$$

(a) *if the series* $\sum_{\mathbf{r}=0}^{\infty}\mathsf{C}_{\mathbf{r}}\,\mathbf{t}^{\mathbf{r}\mathcal{B}}$, $\mathbf{t} \geq 0$ *converges for* $\mathbf{t} = \Lambda$*, then it demonstrates absolute convergence for every real* $\mathbf{t}$ *that meets* $|\mathbf{t}| < |\Lambda|$*,*
(b) *if the series* $\sum_{\mathbf{r}=0}^{\infty}\mathsf{C}_{\mathbf{r}}\,\mathbf{t}^{\mathbf{r}\mathcal{B}}$, $\mathbf{t} \geq 0$ *diverges for* $\mathbf{t} = \Lambda$*, then it demonstrates absolute divergence for every real* $\mathbf{t}$ *that meets* $|\mathbf{t}| > |\Lambda|$*.*

Proof. Given that the series is convergent for $\mathbf{t} = \Lambda$, the series $\sum_{\mathbf{r}=0}^{\infty}\mathsf{C}_{\mathbf{r}}\,\mathbf{t}^{\mathbf{r}\mathcal{B}}$ is convergent for $\mathbf{t} \geq 0$, thus

$$\lim_{\mathbf{r}\longrightarrow\infty}\mathsf{C}_{\mathbf{r}}\,\mathbf{t}^{\mathbf{r}\mathcal{B}} = 0. \tag{4.15}$$

Since, the sequence $\mathsf{C}_{\mathbf{r}}\,\mathbf{t}^{\mathbf{r}\mathcal{B}}$ is convergent, it must be bounded. Thus, there is a positive real number $\mathcal{Q}$ such that $|\mathsf{C}_{\mathbf{r}}\,\mathbf{t}^{\mathbf{r}\mathcal{B}}| \leq \mathcal{Q}$ for all $\mathbf{r} \in \mathcal{N}$. Therefore,

$$|\mathsf{C}_{\mathbf{r}}\,\mathbf{t}^{\mathbf{r}\mathcal{B}}| = |\mathsf{C}_{\mathbf{r}}\,\Lambda^{\mathbf{r}\mathcal{B}}|\left|\frac{\mathbf{t}}{\Lambda}\right|^{\mathbf{r}} \leq \mathcal{Q}\left|\frac{\mathbf{t}}{\Lambda}\right|^{\mathbf{r}}. \tag{4.16}$$

For every $\mathbf{t}$ such that $|\frac{\mathbf{t}}{\Lambda}| < 1$, it follows that $\sum_{\mathbf{r}=0}^{\infty} |\frac{\mathbf{t}}{\Lambda}|^{\mathbf{r}}$ converges for all positive real numbers. By applying the comparison test, the series $\sum_{\mathbf{r}=0}^{\infty} \mathsf{C}_{\mathbf{r}}\, \mathbf{t}^{\mathbf{r}\mathcal{B}}$ converges for $|\mathbf{t}| < |\Lambda|$. This concludes the proof of $(\boldsymbol{a})$.

Let us consider that the fractional power series (4.14) converges when $\mathbf{t} = \mathsf{v}$ provided that $|\Lambda| < |\mathsf{v}|$. Given that the series converges for $\mathbf{t} = \mathsf{v}$ and $|\Lambda| < |\mathsf{v}|$, it follows from $(\boldsymbol{a})$ that the series would also converge when $\mathbf{t} = \Lambda$. This results in a contradiction, implying that the series diverges for every real value of $\mathbf{t}$ where $|\mathbf{t}| > |\Lambda|$. □

Theorem 4.2. *[5] Let $\mathcal{E}$ be an operator that maps $\mathscr{H}$ to $\mathscr{H}$ (where $\mathscr{H}$ is the Hilbert space), and let $\mathscr{X}$ be the precise solution of* (4.1)*. Within this framework, the approximated solution $\sum_{\varrho=0}^{\infty} \Xi_{\varrho}$ converges to $\mathscr{X}$ provided that there is a fixed value σ, (with $0 < \sigma \leq 1$) that satisfies, $\| \Xi_{\varrho+1}(\mathsf{x}, y, \mathbf{t}) \| \leq \sigma \| \Xi_{\varrho}(\mathsf{x}, y, \mathbf{t}) \|$, for every $\varrho \in \mathcal{N} \cup \{0\}$.*

Proof. See reference [5]. □

Now let us apply the previous theory to the proposed model and the solution method to complete the steps of convergence.

Theorem 4.3. *The computed series solution $\mathcal{Z}(\mathsf{x}, y, \mathbf{t}) = \mathcal{Z}_0(\mathsf{x}, y, \mathbf{t}) + \sum_{\iota=1}^{\infty} \mathcal{Z}_{\iota}(\mathsf{x}, y, \mathbf{t})$ is convergent and approaches the precise solution of Eq* (3.1)*.*

Proof. If we assume that, the series solution $\mathcal{Z}(\mathsf{x}, y, \mathbf{t}) = \mathcal{Z}_0(\mathsf{x}, y, \mathbf{t}) + \sum_{\iota=1}^{\infty} \mathcal{Z}_{\iota}(\mathsf{x}, y, \mathbf{t})$ is convergent, then

$$\lim_{\iota \longrightarrow \infty} \mathcal{Z}_{\iota}(\mathsf{x}, y, \mathbf{t}) = 0. \tag{4.17}$$

Since, the truncated series

$$\mathcal{Z}_{\mathcal{M}}(\mathsf{x}, y, \mathbf{t}) = \sum_{\iota=1}^{\mathcal{M}} [\mathcal{Z}_{\iota}(\mathsf{x}, y, \mathbf{t}) - \chi_{\iota} \mathcal{Z}_{\iota-1}(\mathsf{x}, y, \mathbf{t})]. \tag{4.18}$$

Using Eqs (4.17) and (4.18), substituting into (4.11), we obtain

$$\lim_{\mathcal{M} \longrightarrow \infty} \sum_{\iota=1}^{\mathcal{M}} \mathscr{R}_{\iota}(\mathcal{Z}_{\iota-1}^{\rightarrow}(\mathsf{x}, y, \mathbf{t})) = \sum_{\iota=1}^{\infty} \mathscr{R}_{\iota}(\mathcal{Z}_{\iota-1}^{\rightarrow}(\mathsf{x}, y, \mathbf{t})) = 0.$$

Consequently,

$$\begin{aligned} \sum_{\iota=1}^{\infty} \mathscr{R}_{\iota}(\mathcal{Z}_{\iota-1}^{\rightarrow}(\mathsf{x}, y, \mathbf{t})) = \sum_{\iota=1}^{\infty} \Big\{ & J[\mathcal{Z}_{\iota-1}(\mathsf{x}, y, \mathbf{t})](\mathsf{s}, \mathsf{v}) - (1 - \chi_{\iota}) \frac{\mathsf{v}^2}{\mathsf{s}} \mathcal{Z}_0(\mathsf{x}, y, \mathbf{t}) \\ & + \left(\frac{\mathsf{v}}{\mathsf{s}}\right)^{\mathcal{B}} J\Big[- \frac{\partial^2 \mathcal{Z}^2}{\partial \mathsf{x}^2} - \frac{\partial^2 \mathcal{Z}^2}{\partial y^2} - \rho(\mathcal{Z}) \Big] \Big\} \\ & = \left(\frac{\mathsf{v}}{\mathsf{s}}\right)^{\mathcal{B}} J\Big[{}^{C}\mathsf{D}_{\mathbf{t}}^{\mathcal{B}} \mathcal{Z}(\mathsf{x}, y, \mathbf{t}) + \psi(\mathsf{x}, y, \mathbf{t}) - \rho(\mathcal{Z}) \Big], \end{aligned}$$

hence, ${}^{C}\mathsf{D}_{\mathbf{t}}^{\mathcal{B}} \mathcal{Z}(\mathsf{x}, y, \mathbf{t}) + \psi(\mathsf{x}, y, \mathbf{t}) = \rho(\mathcal{Z})$, which confirms that when substituting by the approximated series $\psi(\mathsf{x}, y, \mathbf{t})$ into the series $\mathcal{Z}(\mathsf{x}, y, \mathbf{t}) = \mathcal{Z}_0(\mathsf{x}, y, \mathbf{t}) + \sum_{\iota=1}^{\infty} \mathcal{Z}_{\iota}(\mathsf{x}, y, \mathbf{t})$ this yields the exact solution of the proposed model. □

5. Implementation of the TFNBPM

In this section, we apply the optimal HAJ-TM to solve the TFNBPM under different initial conditions. The overall structure of the model depends on the form of the growth rate function $\rho(\mathcal{Z})$. The general form is

$$ {}^{C}\mathsf{D}_{\mathbf{t}}^{\mathcal{B}}\mathcal{Z}(\mathsf{x}, y, \mathbf{t}) = \frac{\partial^2 \mathcal{Z}^2}{\partial \mathsf{x}^2} + \frac{\partial^2 \mathcal{Z}^2}{\partial y^2} + C\mathcal{Z}^p(1 - r\,\mathcal{Z}^q), \quad 0 < \mathcal{B} \leq 1, \tag{5.1} $$

where C, p, r, and q are constants.

5.1. Malthusian law for growth rate function

In this case, $p = 1$ and $r = 0$, hence, the growth rate function $\rho(\mathcal{Z}) = C\mathcal{Z}$, hence the TFNBPM (5.1) takes the form:

Case I. For the TFNBPM,

$$ {}^{C}\mathsf{D}_{\mathbf{t}}^{\mathcal{B}}\mathcal{Z}(\mathsf{x}, y, \mathbf{t}) = \frac{\partial^2 \mathcal{Z}^2}{\partial \mathsf{x}^2} + \frac{\partial^2 \mathcal{Z}^2}{\partial y^2} + C\mathcal{Z}, \quad 0 < \mathcal{B} \leq 1, \tag{5.2} $$

under initial condition

$$ \mathcal{Z}_0(\mathsf{x}, y, \mathbf{t}) = \mathcal{Z}(\mathsf{x}, y, 0) = \sqrt{\mathsf{x}\, y}. $$

The variables x and y represent spatial coordinates for the two-dimensional population model, where the population or concentration $\mathcal{Z}(\mathsf{x}, y, \mathbf{t})$ changes over time $\mathbf{t}$ and diffuses in both the x and y directions.

To solve Eq (5.2), first, apply JT to both sides,

$$ J[\mathcal{Z}(\mathsf{x}, y, \mathbf{t})](\mathsf{s}, \mathsf{v}) - \frac{\mathsf{v}^2}{\mathsf{s}}\mathcal{Z}_0(\mathsf{x}, y, \mathbf{t}) + \left(\frac{\mathsf{v}}{\mathsf{s}}\right)^{\mathcal{B}} J\Big[- \frac{\partial^2 \mathcal{Z}^2}{\partial \mathsf{x}^2} - \frac{\partial^2 \mathcal{Z}^2}{\partial y^2} - C\mathcal{Z}\Big] = 0, \tag{5.3} $$

when applying the optimal HAJ-TM steps that were discussed in Section 4, we obtain the deformation equation:

$$ \mathcal{Z}_\iota(\mathsf{x}, y, \mathbf{t}) = \chi_\iota \mathcal{Z}_{\iota-1}(\mathsf{x}, y, \mathbf{t}) + \hbar J^{-1}\Big[\mathscr{R}_\iota(\mathcal{Z}_{\iota-1}^{\rightarrow}(\mathsf{x}, y, \mathbf{t}))\Big], \tag{5.4} $$

where

$$ \mathscr{R}_\iota(\mathcal{Z}_{\iota-1}^{\rightarrow}(\mathsf{x}, y, \mathbf{t})) = J[\mathcal{Z}_{\iota-1}](\mathsf{s}, \mathsf{v}) - (1 - \chi_\iota)\frac{\mathsf{v}^2}{\mathsf{s}}\sqrt{\mathsf{x}\, y} + \left(\frac{\mathsf{v}}{\mathsf{s}}\right)^{\mathcal{B}} J\Big[- \frac{\partial^2 \mathcal{Z}_{\iota-1}^2}{\partial \mathsf{x}^2} - \frac{\partial^2 \mathcal{Z}_{\iota-1}^2}{\partial y^2} - C\mathcal{Z}_{\iota-1}\Big]. \tag{5.5} $$

For $\iota = 1$,

$$ \mathcal{Z}_1 = \hbar\, J^{-1}\Big[\mathscr{R}_1(\mathcal{Z}_0)\Big], \tag{5.6} $$

where

$$ \begin{aligned} \mathscr{R}_1(\mathcal{Z}_0) &= J[\mathcal{Z}_0](\mathsf{s}, \mathsf{v}) - \frac{\mathsf{v}^2}{\mathsf{s}}\sqrt{\mathsf{x}\, y} + \left(\frac{\mathsf{v}}{\mathsf{s}}\right)^{\mathcal{B}} J\Big[- \frac{\partial^2 \mathcal{Z}_0^2}{\partial \mathsf{x}^2} - \frac{\partial^2 \mathcal{Z}_0^2}{\partial y^2} - C\mathcal{Z}_0\Big] \\ &= \frac{\mathsf{v}^2}{\mathsf{s}}\sqrt{\mathsf{x}\, y} - \frac{\mathsf{v}^2}{\mathsf{s}}\sqrt{\mathsf{x}\, y} + \left(\frac{\mathsf{v}}{\mathsf{s}}\right)^{\mathcal{B}} J\Big[- C\sqrt{\mathsf{x}y}\Big] \\ &= \left(\frac{\mathsf{v}}{\mathsf{s}}\right)^{\mathcal{B}} \frac{\mathsf{v}^2}{\mathsf{s}}(-C\sqrt{\mathsf{x}y}) \\ &= \frac{\mathsf{v}^{\mathcal{B}+2}}{\mathsf{s}^{\mathcal{B}+1}}(-C\sqrt{\mathsf{x}y}), \end{aligned} \tag{5.7} $$

hence, by taking inverse JT we obtain

$$\mathcal{Z}_1 = \hbar\,(-C\,\sqrt{\mathsf{xy}})\frac{\mathbf{t}^{\mathcal{B}}}{\Gamma(\mathcal{B}+1)}. \tag{5.8}$$

For $\iota = 2$,

$$\mathcal{Z}_2 = \mathcal{Z}_1 + \hbar J^{-1}\Big[\mathscr{R}_2(\mathcal{Z}_1)\Big], \tag{5.9}$$

where

$$\begin{aligned}\mathscr{R}_2(\mathcal{Z}_1) &= J[\mathcal{Z}_1](\mathsf{s},\mathsf{v}) + \left(\frac{\mathsf{v}}{\mathsf{s}}\right)^{\mathcal{B}} J\Big[-\frac{\partial^2\mathcal{Z}_1^2}{\partial\mathsf{x}^2} - \frac{\partial^2\mathcal{Z}_1^2}{\partial y^2} - C\mathcal{Z}_1\Big]\\ &= J\Big[\hbar\,(-C\,\sqrt{\mathsf{xy}})\frac{\mathbf{t}^{\mathcal{B}}}{\Gamma(\mathcal{B}+1)}\Big] + \left(\frac{\mathsf{v}}{\mathsf{s}}\right)^{\mathcal{B}} J\Big[\frac{\hbar C^2\mathbf{t}^{\mathcal{B}}\,\sqrt{\mathsf{xy}}}{\Gamma(\mathcal{B}+1)}\Big]\\ &= \hbar\,(-C\,\sqrt{\mathsf{xy}})\frac{\mathsf{v}^{\mathcal{B}+2}}{\mathsf{s}^{\mathcal{B}+1}} + \left(\frac{\mathsf{v}}{\mathsf{s}}\right)^{\mathcal{B}}\frac{\mathsf{v}^{\mathcal{B}+2}}{\mathsf{s}^{\mathcal{B}+1}}\Big[\hbar C^2\,\sqrt{\mathsf{xy}}\Big]\\ &= \hbar\,(-C\,\sqrt{\mathsf{xy}})\frac{\mathsf{v}^{\mathcal{B}+2}}{\mathsf{s}^{\mathcal{B}+1}} + \frac{\mathsf{v}^{2\mathcal{B}+2}}{\mathsf{s}^{2\mathcal{B}+1}}\Big[\hbar C^2\,\sqrt{\mathsf{xy}}\Big].\end{aligned} \tag{5.10}$$

Hence,

$$\begin{aligned}\mathcal{Z}_2 &= \mathcal{Z}_1 + \hbar J^{-1}\Big[\hbar\,(-C\,\sqrt{\mathsf{xy}})\frac{\mathsf{v}^{\mathcal{B}+2}}{\mathsf{s}^{\mathcal{B}+1}} + \frac{\mathsf{v}^{2\mathcal{B}+2}}{\mathsf{s}^{2\mathcal{B}+1}}\Big(\hbar C^2\,\sqrt{\mathsf{xy}}\Big)\Big]\\ &= \hbar\,(-C\,\sqrt{\mathsf{xy}})\frac{\mathbf{t}^{\mathcal{B}}}{\Gamma(\mathcal{B}+1)} + \hbar^2\,(-C\,\sqrt{\mathsf{xy}})\frac{\mathbf{t}^{\mathcal{B}}}{\Gamma(\mathcal{B}+1)} + (\hbar^2\,C^2\,\sqrt{\mathsf{xy}})\frac{\mathbf{t}^{2\mathcal{B}}}{\Gamma(2\mathcal{B}+1)}.\end{aligned} \tag{5.11}$$

By setting $\iota = 3, 4, ...$, and using "Mathematica 13.2" software, we can easily evaluate $\mathcal{Z}_3, \mathcal{Z}_4, ...$ The approximate solution will be

$$\mathcal{Z}(\mathsf{x}, y, \mathbf{t}) = \mathcal{Z}_0 + \mathcal{Z}_1 + \mathcal{Z}_2 + \mathcal{Z}_3 + ... \tag{5.12}$$

Table 1 clarifies the exact and estimated solutions obtained from solving the TFNBPM Case I under initial condition $\mathcal{Z}_0 = \sqrt{\mathsf{xy}}$ at $\mathcal{B} = 1$ and $C = 0.5$ for $y = 2$ and $\hbar = -1$ for several values of x once at $\mathbf{t} = 0.1$, other at $\mathbf{t} = 0.2$, and at $\mathbf{t} = 1$. These values result from expanding six approximated terms. The results are excellent, which reflect the efficiency of the JT when applied with the optimal HAM.

Table 1. The exact and the estimated solutions for the TFNBPM **Case I** under initial condition $\mathcal{Z}_0 = \sqrt{\mathrm{x}y}$ at $\mathcal{B} = 1$ and $C = 0.5$ for $y = 2$ and $\hbar = -1$.

t	x	Exact Sol.	Est. Sol.	$\lvert Error\rvert$
	-8	4.20508	4.20508	6.24389×10^{-13}
	-5	3.32441	3.32441	4.93383×10^{-13}
	-2	2.10254	2.10254	3.12195×10^{-13}
0.1	1	1.48672	1.48672	2.20490×10^{-13}
	4	2.97344	2.97344	4.40981×10^{-13}
	7	3.93350	3.93350	5.83977×10^{-13}
	10	4.70143	4.70143	6.98108×10^{-13}
	-8	4.42068	4.42068	8.03686×10^{-11}
	-5	3.49486	3.49486	6.35367×10^{-11}
0.2	-2	2.21034	2.21034	4.01843×10^{-11}
	1	1.56295	1.56295	2.84146×10^{-11}
	4	3.12590	3.12590	5.68292×10^{-11}
	7	4.13517	4.13517	7.51781×10^{-11}
	10	4.94247	4.94247	8.98552×10^{-11}
	-8	6.59489	6.59488	6.61058×10^{-6}
	-5	5.21371	5.21371	5.22612×10^{-6}
1	-2	3.29744	3.29744	3.30529×10^{-6}
	1	2.33164	2.33164	2.33719×10^{-6}
	4	4.66329	4.66328	4.67438×10^{-6}
	7	6.16895	6.16894	6.18363×10^{-6}
	10	7.37331	7.373310	7.39085×10^{-6}

As we mentioned before, the parameter $\hbar$ controls the convergence of the solution. From Figure 3, it is clear that the region in which the fast convergence exists is the area aligned with the $x - axis$ and it usually includes the value -1. But if we want to ascertain the exact value of $\hbar$ that gives an optimal solution, we calculate the average residual error presented in Eq (4.13) and minimize its value.

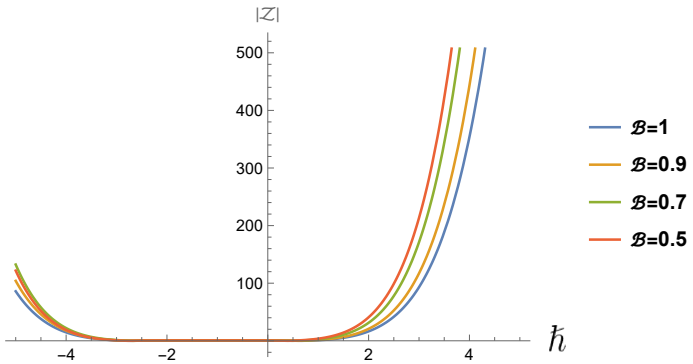

Figure 3. The $\hbar$-curves of the TFNBPM (Malthusian law Case I) at $C = 0.5, \mathrm{x} = 0.5, y = 0.5$, and $\mathbf{t} = 0.1$ for different $\mathcal{B}$ values.

Table 2 presents the values of $\hbar$ that gives optimal solutions and the corresponding $\mathcal{E}(\hbar)$ at different $\mathcal{B}$ values. The values of $\hbar$ matches with the region of convergence that appears in Figure 3.

Table 2. The optimal value $\hbar$ and its corresponding average residual error at several $\mathcal{B}$ values when $C = 0.5$.

$\mathcal{B}$	$\hbar$- Optimal	The average residual error $\mathcal{E}(\hbar)$
1.0	-1.05205	5.09710 E-38
0.8	-1.16722	2.74219 E-37
0.6	-1.26108	9.70729 E-35
0.4	-1.27654	1.09485 E-32

It is worth noting that, the series solution (5.12) that introduces the estimated solution, if we substitute by $\hbar = -1$, we obtain

$$\mathcal{Z}(\mathsf{x}, y, \mathbf{t}) = \sqrt{\mathsf{x}y} + C\sqrt{\mathsf{x}y}\frac{\mathbf{t}^{\mathcal{B}}}{\Gamma(\mathcal{B}+1)} + C^2\sqrt{\mathsf{x}y}\frac{\mathbf{t}^{2\mathcal{B}}}{\Gamma(2\mathcal{B}+1)} + ... = \sqrt{\mathsf{x}y}\sum_{v=0}^{\infty} C^v \frac{\mathbf{t}^{v\mathcal{B}}}{\Gamma(v\mathcal{B}+1)},$$

which is the same solution obtained by Vineet Srivastava et al. in [24], when solved by the fractional reduced differential transform method. And the same results obtained by Yanqin Liu et al. in [36] at $\mathcal{B} = 1$.

To clarify that obtaining the optimal parameter $\hbar$ improves the accuracy of the solution, we present Table 3, which represents the absolute error at $\mathcal{B} = 1$ for HAM with JT and for optimal HAJ-TM with fixed values for $\mathsf{x} = y = 2$ and different values of $\mathbf{t}$.

Table 3. Comparison between the HAM with JT and optimal HAJ-TM at $\mathsf{x} = y = 2$ at $\mathcal{B} = 1$ and $C = 0.5$.

$\mathbf{t}$	Abs. error HAM with JT at $\hbar = -1$	Abs. error HAM with JT at $\hbar = -0.9$	Abs. error of optimal HAJ-TM at $\hbar$ optimal $= -1.05832$
0.1	3.12195 E-13	2.99288 E-7	4.46216 E-16
0.2	4.01839 E-11	1.32580 E-6	3.27812 E-16
0.3	6.90941 E-10	3.79505 E-6	1.53273 E-15
0.4	5.20923 E-9	8.79792 E-6	4.45890 E-15

In this case, when evaluating the minimal average residual error at $\hbar$ optimal $= -1.05832$, it becomes $2.22242E-36$, which confirms that we can obtain an optimal solution by obtaining $\hbar$ optimal value.

Case II. For the TFNBPM,

$$^{C}\mathsf{D}_{\mathbf{t}}^{\mathcal{B}}\mathcal{Z}(\mathsf{x}, y, \mathbf{t}) = \frac{\partial^2\mathcal{Z}^2}{\partial\mathsf{x}^2} + \frac{\partial^2\mathcal{Z}^2}{\partial y^2} + C\mathcal{Z}, \quad 0 < \mathcal{B} \leq 1, \ \mathbf{t} \geq 0, \tag{5.13}$$

under initial condition

$$\mathcal{Z}_0(\mathsf{x}, y, \mathbf{t}) = \mathcal{Z}(\mathsf{x}, y, 0) = \sqrt{sin\mathsf{x}\ sinhy}.$$

By applying the same steps of **Case I**, one can obtain

$$\mathcal{Z}_1 = \hbar\,(-C\,\sqrt{sin\mathsf{x}\,sinhy})\frac{\mathbf{t}^{\mathcal{B}}}{\Gamma(\mathcal{B}+1)}. \tag{5.14}$$

$$\mathcal{Z}_2 = (1+\hbar)\mathcal{Z}_1 + \hbar^2(C^2\,\sqrt{sin\mathsf{x}\,sinhy})\frac{\mathbf{t}^{2\mathcal{B}}}{\Gamma(2\mathcal{B}+1)}. \tag{5.15}$$

$$\mathcal{Z}_3 = (1+\hbar)\mathcal{Z}_2 + \hbar^2(1+\hbar)(C^2\,\sqrt{sin\mathsf{x}\,sinhy})\frac{\mathbf{t}^{2\mathcal{B}}}{\Gamma(2\mathcal{B}+1)} - \hbar^3(C^3\,\sqrt{sin\mathsf{x}\,sinhy})\frac{\mathbf{t}^{3\mathcal{B}}}{\Gamma(3\mathcal{B}+1)}. \tag{5.16}$$

Again, using "Mathematica 13.2" software, we can easily calculate $\mathcal{Z}_4, \mathcal{Z}_5, ...$ Hence the approximated solution in the form of a series will be

$$\mathcal{Z}(\mathsf{x}, y, \mathbf{t}) = \mathcal{Z}_0 + \mathcal{Z}_1 + \mathcal{Z}_2 + \mathcal{Z}_3 + \mathcal{Z}_4 + ... \tag{5.17}$$

Table 4 represents the precise and the calculated solutions for the TFNBPM Case I for $\mathcal{Z}_0 = \sqrt{sin\mathsf{x}\,sinhy}$ initial guess at $\mathcal{B} = 1$ and $C = 0.25$ for $y = 2$ and $\hbar = -1$ at $\mathbf{t} = 0.1$, $\mathbf{t} = 0.2$, and at $\mathbf{t} = 1$. These values result from expanding 6 terms ($\mathcal{Z}_0 + \mathcal{Z}_1 + \mathcal{Z}_2 + ... + \mathcal{Z}_5$). The results are excellent since they produce a very small error, which clarifies the efficiency of applying the optimal HAJ-TM.

Table 4. The exact and the estimated solutions for the TFNBPM **Case I** under initial condition $\mathcal{Z}_0 = \sqrt{sin\mathsf{x}\,sinhy}$ at $\mathcal{B} = 1$ and $C = 0.25$ for $y = 2$ and $\hbar = -1$.

t	x	Exact Sol.	Est. Sol.	$\lvert Error\rvert$
	-8	1.94223	1.94223	2.44249×10^{-15}
	-5	1.91212	1.91212	2.44249×10^{-15}
	-2	1.86198	1.86198	2.22045×10^{-15}
0.1	1	1.79119	1.79119	2.22045×10^{-15}
	4	1.69869	1.69869	1.99840×10^{-15}
	7	1.58271	1.58271	1.99840×10^{-15}
	10	1.44023	1.44023	1.77636×10^{-15}
	-8	1.99139	1.99139	2.95541×10^{-13}
	-5	1.96052	1.96052	2.91100×10^{-13}
0.2	-2	1.90912	1.90912	2.83329×10^{-13}
	1	1.83654	1.83654	2.72671×10^{-13}
	4	1.74169	1.74169	2.58682×10^{-13}
	7	1.62278	1.62278	2.40918×10^{-13}
	10	1.47669	1.47669	2.19158×10^{-13}
	-8	2.43229	2.43229	2.36772×10^{-8}
	-5	2.39459	2.39459	2.33102×10^{-8}
1	-2	2.33180	2.33180	2.26990×10^{-8}
	1	2.24315	2.24315	2.18360×10^{-8}
	4	2.12731	2.12731	2.07083×10^{-8}
	7	1.98206	1.98206	1.92944×10^{-8}
	10	1.80363	1.80363	1.75575×10^{-8}

Figure 4 represents the $\hbar$-curves at various $\mathcal{B}$ values; it is clear that the region in which the fast convergence exists is approximately $[-2.5, 0.5]$. To ascertain the particular value of $\hbar$ that gives an optimal solution, we calculate the average residual error presented in Eq (4.13) and minimize its value. The values of optimal $\hbar$ and its corresponding error are presented in Table 5.

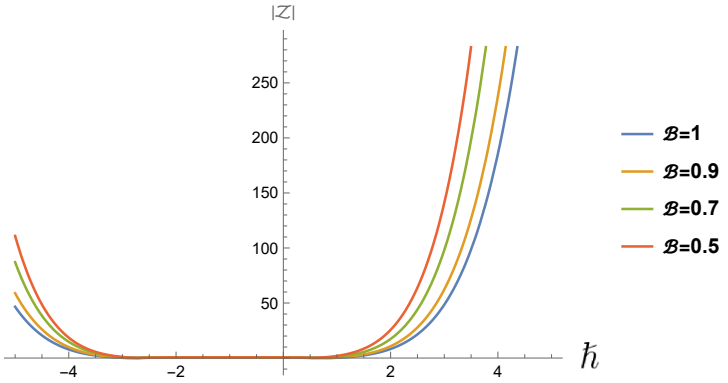

Figure 4. The $\hbar$-curves of the TFNBPM (Malthusian law Case II) at $C = 0.25, \mathsf{x} = 0.5$, $y = 0.5$ and $\mathbf{t} = 0.1$ for various $\mathcal{B}$ values.

Table 5. The optimal value $\hbar$ and its corresponding average residual error at several $\mathcal{B}$ values when $C = 0.25$.

$\mathcal{B}$	The optimal value of $\hbar$	The average residual error $\mathcal{E}(\hbar)$
1.0	-1.05037	1.74892 E-39
0.8	-1.04323	7.72337 E-38
0.6	-1.11547	7.95951 E-37
0.4	-1.16775	1.34901 E-35

By noticing the approximated solution obtained, when substituting by $\hbar = -1$, the solution takes the form:

$$\begin{aligned}\mathcal{Z}(\mathsf{x}, y, \mathbf{t}) &= \sqrt{sin\mathsf{x}\, sinhy} + C\sqrt{sin\mathsf{x}\, sinhy}\frac{\mathbf{t}^{\mathcal{B}}}{\Gamma(\mathcal{B}+1)} + C^2\sqrt{sin\mathsf{x}\, sinhy}\frac{\mathbf{t}^{2\mathcal{B}}}{\Gamma(2\mathcal{B}+1)} + \ldots \\ &= \sqrt{sin\mathsf{x}\, sinhy}\sum_{v=0}^{\infty} C^v \frac{\mathbf{t}^{v\mathcal{B}}}{\Gamma(v\mathcal{B}+1)}.\end{aligned}$$

This is the same solution obtained by Vineet Srivastava et al. in [24] and also the same solution obtained by Mohammad Alaroud et al. in [28] when they solved the system using the residual power series method.

5.2. *Verhulst law for growth rate function*

In this case, if we put $C = p = q = 1$, in Eq (5.1), the growth rate function $\rho(\mathcal{Z}) = \mathcal{Z}(1 - r\mathcal{Z})$, hence the TFNBPM takes the form:

$$^{C}\mathsf{D}_{\mathbf{t}}^{\mathcal{B}}\mathcal{Z}(\mathsf{x}, y, \mathbf{t}) = \frac{\partial^2\mathcal{Z}^2}{\partial\mathsf{x}^2} + \frac{\partial^2\mathcal{Z}^2}{\partial y^2} + \mathcal{Z}(1 - r\mathcal{Z}), \quad 0 < \mathcal{B} \leq 1, \tag{5.18}$$

with initial condition

$$\mathcal{Z}_0(\mathsf{x}, y, \mathbf{t}) = e^{\frac{1}{2}\sqrt{\frac{r}{2}}(\mathsf{x}+y)}.$$

Applying the optimal HAJ-TM steps presented in Section 4, we obtain the deformation equation:

$$\mathcal{Z}_\iota(\mathsf{x}, y, \mathbf{t}) = \chi_\iota \mathcal{Z}_{\iota-1}(\mathsf{x}, y, \mathbf{t}) + \hbar J^{-1}\Big[\mathscr{R}_\iota(\mathcal{Z}^{\rightarrow}_{\iota-1}(\mathsf{x}, y, \mathbf{t}))\Big], \tag{5.19}$$

where

$$\mathscr{R}_\iota(\mathcal{Z}^{\rightarrow}_{\iota-1}) = J[\mathcal{Z}_{\iota-1}] - (1-\chi_\iota)\frac{\mathsf{v}^2}{\mathsf{s}}e^{\frac{1}{2}\sqrt{\frac{r}{2}}(\mathsf{x}+y)} + \left(\frac{\mathsf{v}}{\mathsf{s}}\right)^{\mathcal{B}} J\Big[-\frac{\partial^2\mathcal{Z}^2_{\iota-1}}{\partial\mathsf{x}^2} - \frac{\partial^2\mathcal{Z}^2_{\iota-1}}{\partial y^2} - \mathcal{Z}_{\iota-1}(1-r\mathcal{Z}_{\iota-1})\Big]. \tag{5.20}$$

When $\iota = 1$,

$$\mathcal{Z}_1 = \hbar\, J^{-1}\Big[\mathscr{R}_1(\mathcal{Z}_0)\Big], \tag{5.21}$$

where

$$\begin{aligned}
\mathscr{R}_1(\mathcal{Z}_0) &= J(\mathcal{Z}_0) - \frac{\mathsf{v}^2}{\mathsf{s}}e^{\frac{1}{2}\sqrt{\frac{r}{2}}(\mathsf{x}+y)} + \left(\frac{\mathsf{v}}{\mathsf{s}}\right)^{\mathcal{B}} J\Big[-\frac{\partial^2\mathcal{Z}^2_0}{\partial\mathsf{x}^2} - \frac{\partial^2\mathcal{Z}^2_0}{\partial y^2} - \mathcal{Z}_0(1-r\mathcal{Z}_0)\Big] \\
&= \frac{\mathsf{v}^2}{\mathsf{s}}e^{\frac{1}{2}\sqrt{\frac{r}{2}}(\mathsf{x}+y)} - \frac{\mathsf{v}^2}{\mathsf{s}}e^{\frac{1}{2}\sqrt{\frac{r}{2}}(\mathsf{x}+y)} + \left(\frac{\mathsf{v}}{\mathsf{s}}\right)^{\mathcal{B}} J\Big[-e^{\frac{\sqrt{r}(\mathsf{x}+y)}{2\sqrt{2}}}\Big] \\
&= \left(\frac{\mathsf{v}}{\mathsf{s}}\right)^{\mathcal{B}}\frac{\mathsf{v}^2}{\mathsf{s}}(-e^{\frac{\sqrt{r}(\mathsf{x}+y)}{2\sqrt{2}}}) \\
&= \frac{\mathsf{v}^{\mathcal{B}+2}}{\mathsf{s}^{\mathcal{B}+1}}(-e^{\frac{\sqrt{r}(\mathsf{x}+y)}{2\sqrt{2}}}).
\end{aligned} \tag{5.22}$$

Taking inverse JT to obtain,

$$\mathcal{Z}_1 = \hbar\,(-e^{\frac{\sqrt{r}(\mathsf{x}+y)}{2\sqrt{2}}})\frac{\mathbf{t}^{\mathcal{B}}}{\Gamma(\mathcal{B}+1)}. \tag{5.23}$$

When $\iota = 2$,

$$\mathcal{Z}_2 = \mathcal{Z}_1 + \hbar J^{-1}\Big[\mathscr{R}_2(\mathcal{Z}_1)\Big], \tag{5.24}$$

where,

$$\begin{aligned}
\mathscr{R}_2(\mathcal{Z}_1) &= J[\mathcal{Z}_1] + \left(\frac{\mathsf{v}}{\mathsf{s}}\right)^{\mathcal{B}} J\Big[-\frac{\partial^2\mathcal{Z}^2_1}{\partial\mathsf{x}^2} - \frac{\partial^2\mathcal{Z}^2_1}{\partial y^2} - \mathcal{Z}_1(1-r\mathcal{Z}_1)\Big] \\
&= J\Big[\hbar\,(-e^{\frac{\sqrt{r}(\mathsf{x}+y)}{2\sqrt{2}}})\frac{\mathbf{t}^{\mathcal{B}}}{\Gamma(\mathcal{B}+1)}\Big] + \left(\frac{\mathsf{v}}{\mathsf{s}}\right)^{\mathcal{B}} J\Big[\frac{\hbar\mathbf{t}^{\mathcal{B}}e^{\frac{\sqrt{r}(\mathsf{x}+y)}{2\sqrt{2}}}}{\Gamma(\mathcal{B}+1)}\Big] \\
&= \hbar\,(-e^{\frac{\sqrt{r}(\mathsf{x}+y)}{2\sqrt{2}}})\frac{\mathsf{v}^{\mathcal{B}+2}}{\mathsf{s}^{\mathcal{B}+1}} + \left(\frac{\mathsf{v}}{\mathsf{s}}\right)^{\mathcal{B}}\Big[\hbar e^{\frac{\sqrt{r}(\mathsf{x}+y)}{2\sqrt{2}}}\frac{\mathsf{v}^{\mathcal{B}+2}}{\mathsf{s}^{\mathcal{B}+1}}\Big].
\end{aligned} \tag{5.25}$$

Then, by substituting in Eq (5.24),

$$\begin{aligned}
\mathcal{Z}_2 &= \mathcal{Z}_1 + \hbar J^{-1}\Big\{\hbar\,(-e^{\frac{\sqrt{r}(\mathsf{x}+y)}{2\sqrt{2}}})\frac{\mathsf{v}^{\mathcal{B}+2}}{\mathsf{s}^{\mathcal{B}+1}} + \left(\frac{\mathsf{v}}{\mathsf{s}}\right)^{\mathcal{B}}\Big[\hbar e^{\frac{\sqrt{r}(\mathsf{x}+y)}{2\sqrt{2}}}\frac{\mathsf{v}^{\mathcal{B}+2}}{\mathsf{s}^{\mathcal{B}+1}}\Big]\Big\} \\
&= \mathcal{Z}_1 + \hbar^2\,(-e^{\frac{\sqrt{r}(\mathsf{x}+y)}{2\sqrt{2}}})\frac{\mathbf{t}^{\mathcal{B}}}{\Gamma(\mathcal{B}+1)} + \hbar^2\,(e^{\frac{\sqrt{r}(\mathsf{x}+y)}{2\sqrt{2}}})\frac{\mathbf{t}^{2\mathcal{B}}}{\Gamma(2\mathcal{B}+1)} \\
&= \mathcal{Z}_1(1+\hbar) + \hbar^2\,(e^{\frac{\sqrt{r}(\mathsf{x}+y)}{2\sqrt{2}}})\frac{\mathbf{t}^{2\mathcal{B}}}{\Gamma(2\mathcal{B}+1)}.
\end{aligned} \tag{5.26}$$

When $\iota = 3$,

$$\mathcal{Z}_3 = \mathcal{Z}_2 + \hbar J^{-1}\Big[\mathscr{R}_3(\mathcal{Z}_2)\Big], \tag{5.27}$$

where,

$$\begin{aligned}\mathscr{R}_3(\mathcal{Z}_2) &= J[\mathcal{Z}_2] + \left(\frac{\mathsf{v}}{\mathsf{s}}\right)^{\mathcal{B}} J\Big[-\frac{\partial^2\mathcal{Z}_2^2}{\partial \mathsf{x}^2} - \frac{\partial^2\mathcal{Z}_2^2}{\partial y^2} - \mathcal{Z}_2(1 - r\mathcal{Z}_2)\Big] \\ &= J(\mathcal{Z}_2) + \left(\frac{\mathsf{v}}{\mathsf{s}}\right)^{\mathcal{B}} J\Big[-\frac{\hbar^2\mathbf{t}^{2\mathcal{B}} e^{\frac{\sqrt{r}(\mathsf{x}+y)}{2\sqrt{2}}}}{\Gamma(2\mathcal{B}+1)} + \frac{\hbar^2\mathbf{t}^{\mathcal{B}} e^{\frac{\sqrt{r}(\mathsf{x}+y)}{2\sqrt{2}}}}{\Gamma(\mathcal{B}+1)} + \frac{\hbar\mathbf{t}^{\mathcal{B}} e^{\frac{\sqrt{r}(\mathsf{x}+y)}{2\sqrt{2}}}}{\Gamma(\mathcal{B}+1)}\Big] \\ &= J(\mathcal{Z}_2) + \left(\frac{\mathsf{v}}{\mathsf{s}}\right)^{\mathcal{B}}\Big[-\hbar^2 e^{\frac{\sqrt{r}(\mathsf{x}+y)}{2\sqrt{2}}}\frac{\mathsf{v}^{2\mathcal{B}+2}}{\mathsf{s}^{2\mathcal{B}+1}} + \Big(\hbar^2 e^{\frac{\sqrt{r}(\mathsf{x}+y)}{2\sqrt{2}}} + \hbar e^{\frac{\sqrt{r}(\mathsf{x}+y)}{2\sqrt{2}}}\Big)\frac{\mathsf{v}^{\mathcal{B}+2}}{\mathsf{s}^{\mathcal{B}+1}}\Big].\end{aligned} \tag{5.28}$$

Then, by substituting in Eq (5.27),

$$\begin{aligned}\mathcal{Z}_3 &= \mathcal{Z}_2 + \hbar J^{-1}\Big\{J(\mathcal{Z}_2) + \left(\frac{\mathsf{v}}{\mathsf{s}}\right)^{\mathcal{B}}\Big[-\hbar^2 e^{\frac{\sqrt{r}(\mathsf{x}+y)}{2\sqrt{2}}}\frac{\mathsf{v}^{2\mathcal{B}+2}}{\mathsf{s}^{2\mathcal{B}+1}} + \Big(\hbar^2 e^{\frac{\sqrt{r}(\mathsf{x}+y)}{2\sqrt{2}}} + \hbar e^{\frac{\sqrt{r}(\mathsf{x}+y)}{2\sqrt{2}}}\Big)\frac{\mathsf{v}^{\mathcal{B}+2}}{\mathsf{s}^{\mathcal{B}+1}}\Big]\Big\} \\ &= \mathcal{Z}_2 + \hbar\,\mathcal{Z}_2 + \hbar^3(-e^{\frac{\sqrt{r}(\mathsf{x}+y)}{2\sqrt{2}}})\frac{\mathbf{t}^{3\mathcal{B}}}{\Gamma(3\mathcal{B}+1)} + \Big(\hbar^3 e^{\frac{\sqrt{r}(\mathsf{x}+y)}{2\sqrt{2}}} + \hbar^2 e^{\frac{\sqrt{r}(\mathsf{x}+y)}{2\sqrt{2}}}\Big)\frac{\mathbf{t}^{2\mathcal{B}}}{\Gamma(2\mathcal{B}+1)} \\ &= \mathcal{Z}_2(1+\hbar) + \Big(\hbar^3 e^{\frac{\sqrt{r}(\mathsf{x}+y)}{2\sqrt{2}}} + \hbar^2 e^{\frac{\sqrt{r}(\mathsf{x}+y)}{2\sqrt{2}}}\Big)\frac{\mathbf{t}^{2\mathcal{B}}}{\Gamma(2\mathcal{B}+1)} + \hbar^3(-e^{\frac{\sqrt{r}(\mathsf{x}+y)}{2\sqrt{2}}})\frac{\mathbf{t}^{3\mathcal{B}}}{\Gamma(3\mathcal{B}+1)}.\end{aligned} \tag{5.29}$$

And so on, setting $\iota = 4, 5, ...$, and using "Mathematica 13.2" software, we can easily evaluate $\mathcal{Z}_4, \mathcal{Z}_5, ...$ The approximate solution will be

$$\mathcal{Z}(\mathsf{x}, y, \mathbf{t}) = \mathcal{Z}_0 + \mathcal{Z}_1 + \mathcal{Z}_2 + \mathcal{Z}_3 + ... \tag{5.30}$$

Table 6 shows the precise, calculated solutions, and the absolute error between the two, that results from solving the TFNBPM for the Verhulst law of population growth at $\mathcal{B} = 1$ and $r = 0.5$ for $y = 2$ and $\hbar = -1$. The results shown in the table for the calculated solution are obtained by expanding six terms. The accuracy of the solution increases with the number of terms expanded, which confirms the convergence of the series representing the solution we obtained.

As we did in previous cases to determine the region where the solution achieves faster convergence, we graph the $\hbar$-curves. The area aligned with the $x-axis$ is where the solution converges more quickly. The common value of $\hbar$ that is included in the region of convergence is -1 and this matches with the region that appears in Figure 5.

By noticing the series solution (5.30), if we substitute by $\hbar = -1$, we obtain a closed form solution:

$$\begin{aligned}\mathcal{Z}(\mathsf{x}, y, \mathbf{t}) &= e^{\frac{\sqrt{r}(\mathsf{x}+y)}{2\sqrt{2}}} + e^{\frac{\sqrt{r}(\mathsf{x}+y)}{2\sqrt{2}}}\frac{\mathbf{t}^{\mathcal{B}}}{\Gamma(\mathcal{B}+1)} + e^{\frac{\sqrt{r}(\mathsf{x}+y)}{2\sqrt{2}}}\frac{\mathbf{t}^{2\mathcal{B}}}{\Gamma(2\mathcal{B}+1)} + ... \\ &= e^{\frac{\sqrt{r}(\mathsf{x}+y)}{2\sqrt{2}}}\sum_{\nu=0}^{\infty}\frac{\mathbf{t}^{\nu\mathcal{B}}}{\Gamma(\nu\mathcal{B}+1)},\end{aligned}$$

which is the same solution obtained by Mohammad Alaroud et al. in [28], when they solved the system using the residual power series method.

From the results shown in the tables, it is clear that using the JT with the optimal HAM provides very good results for solving fractional differential equations.

Table 6. The exact and calculated solutions for the TFNBPM for Verhulst law of population growth at $\mathcal{B} = 1$ and $r = 0.5$ for $y = 2$ and $\hbar = -1$.

t	x	Exact Sol.	Est. Sol.	$\lvert Error\rvert$
	-8	0.246597	0.246597	4.48316×10^{-12}
	-5	0.522046	0.522046	9.49085×10^{-12}
	-2	1.105170	1.105170	2.00919×10^{-11}
0.1	1	2.339650	2.339650	4.25344×10^{-11}
	4	4.953030	4.953030	9.00471×10^{-11}
	7	10.48560	10.48560	1.90628×10^{-10}
	10	22.19800	22.19800	4.03563×10^{-10}
	-8	0.272532	0.272532	5.81168×10^{-10}
	-5	0.576950	0.576950	1.23033×10^{-9}
0.2	-2	1.221400	1.221400	2.60461×10^{-9}
	1	2.585710	2.585710	5.51397×10^{-9}
	4	5.473950	5.473950	1.16731×10^{-8}
	7	11.58830	11.58830	2.47119×10^{-8}
	10	24.53250	24.53250	5.23151×10^{-8}

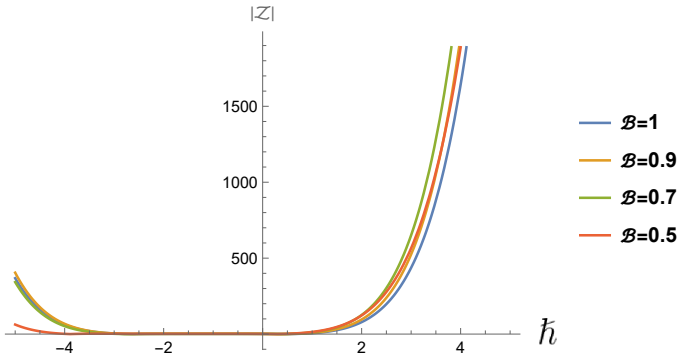

Figure 5. The $\hbar$-curves of the TFNBPM ((Verhulst law for population) at $r = 0.5, \mathrm{x} = 0.5$, $y = 0.5$, and $\mathbf{t} = 0.1$ for various $\mathcal{B}$ values.

To confirm the accuracy of our results, Let us present Tables 7 and 8, which present comparisons between the results we obtained for Malthusian and Verhulst growth with one of the efficient semi-analytical methods, which is the Laplace fractional power series method presented in [28]. We recorded the results at the same parameter values and the same number of expanded terms.

Table 7. Comparisons between our results and the results presented in [28] using absolute error values for the TFNBPM at the same parameter values for Malthusian growth.

Case I Eq (5.2) for $C = 0.5$ at $(\mathsf{x}, y) = (2, 3)$			Case II Eq (5.13) for $C = 0.1$at $(\mathsf{x}, y) = (1, 30)$		
t	The Abs. error presented in [28]	The Abs. error of our results at $\hbar = -1.05$	**t**	The Abs. error presented in [28]	The Abs. error of our results at $\hbar = -1.05$
0.5	3.061708×10^{-8}	6.15423×10^{-9}	1	1.080055×10^{-9}	3.70520×10^{-10}
1	4.048135×10^{-6}	7.05123×10^{-8}	2	7.013444×10^{-8}	1.32080×10^{-8}
1.5	7.150407×10^{-5}	1.38533×10^{-6}	3	8.106860×10^{-7}	9.65756×10^{-8}
2	5.542531×10^{-4}	1.80585×10^{-5}	4	4.623050×10^{-6}	1.21562×10^{-8}
2.5	2.736956×10^{-3}	3.24755×10^{-4}	5	1.790206×10^{-5}	9.26610×10^{-7}
3	1.016540×10^{-2}	2.12395×10^{-3}	6	5.427211×10^{-5}	2.15195×10^{-6}

Table 8. Comparisons between our results and the results presented in [28] using absolute error values for the TFNBPM at the same parameter values for Verhulst growth.

Verhulst growth Eq (5.18) at $r = 0.5$ and $(\mathsf{x}, y) = (1, 1)$		
t	The Abs. error presented in [28]	The Abs. error of our results at $\hbar = -1.05$
0.32	1.154399×10^{-5}	1.78803×10^{-7}
0.64	7.752680×10^{-4}	2.84184×10^{-6}
0.96	9.282582×10^{-3}	2.83280×10^{-4}
1.28	5.492411×10^{-2}	3.56900×10^{-3}
1.6	2.210639×10^{-1}	2.04997×10^{-2}
1.92	6.978720×10^{-1}	7.99154×10^{-2}

6. Graphical illustrations

Graphs are the main tool that provides an explanation about the system dynamics and also shows the effects of all parameters about each other in a simple way. In this study, we presented two- and three-dimensional graphs of all solutions we obtained. Figure 6 represents the 2D profile of solving the TFNBPM presented in Eq (5.2) at $C = 0.5$ and $\hbar = -1$. Figure 6(a) introduces the solution at $\mathsf{x} = 2$, and $y = 3$ for different fractional order derivatives $\mathcal{B}$, while Figure 6(b) introduces the solution at $y = 3$ and several time steps. Figure 7 clarifies the 3D solution of the TFNBPM (5.2); Figure 7(a) clarifies the obtained calculated solution; and Figure 7(b) clarifies the exact solution; the two graphs provide matching between them. Figure 8 provides a two-dimensional interface for the solution of TFNBPM (5.13) at $C = 0.25$ and $\hbar = -1$. Also this figure has two profiles, one at different $\mathcal{B}$-values and the other at different time values. Figure 9 is the three-dimensional profile of the TFNBPM (5.13) which gives soliton wave shapes; Figure 9(a) is the approximated solution at $\mathcal{B} = 1$, and Figure 9(b) is the exact solution. Figure 10 represents the TFNBPM (5.18) in 2D; Figure 10(a) is the solution at $\mathsf{x} = 2, y = 3$, $r = 0.5$ and $\hbar = -1$. Figure 10(b) is the solution at $y = 3$ for several time steps. Figure 11 is the 3D profile for the approximate and the exact solution at the same parameters of TFNBPM (5.18). From the figures represented, especially the three-dimensional figures, we notice a great similarity between the

solutions we obtained and the accurate solutions, this reflects the efficiency of the applied technique for solution.

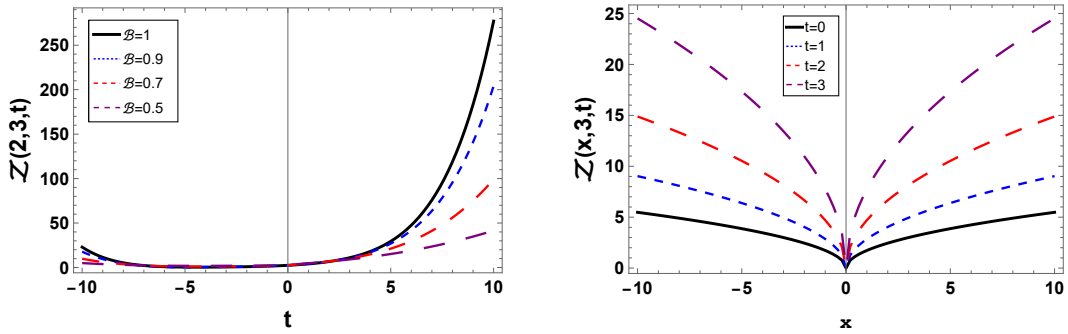

Figure 6. Two-dimensional solution profile presented in Eq (5.12) at $C = 0.5$ and $\hbar = -1$. (a) For $\mathrm{x} = 2, y = 3$ for various $\mathcal{B}$ values; (b) For $y = 3$ and several time steps.

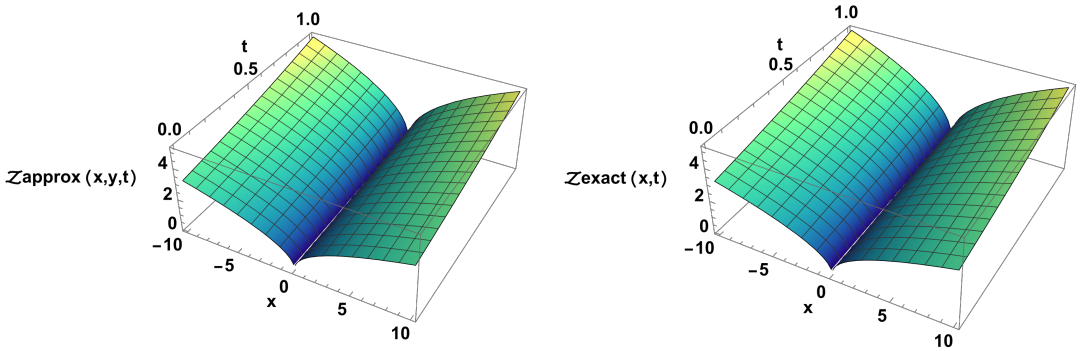

Figure 7. 3D depiction of the solution to the TFNBPM at $y = 1$. (a) The estimated solution from Eq (5.12) at $\mathcal{B} = 1$; (b) the exact solution.

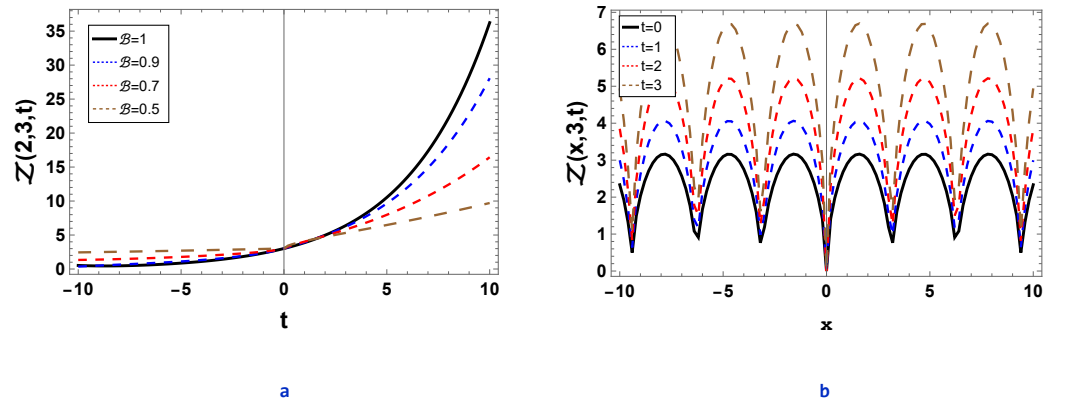

Figure 8. Two-dimensional solution profile of TFNBPM (second case of Malthusian law for population) presented in Eq (5.17) at $C = 0.25$ and $\hbar = -1$. (a) For $\mathrm{x} = 2, y = 3$ for various $\mathcal{B}$ values; (b) for $y = 3$ and several time steps.

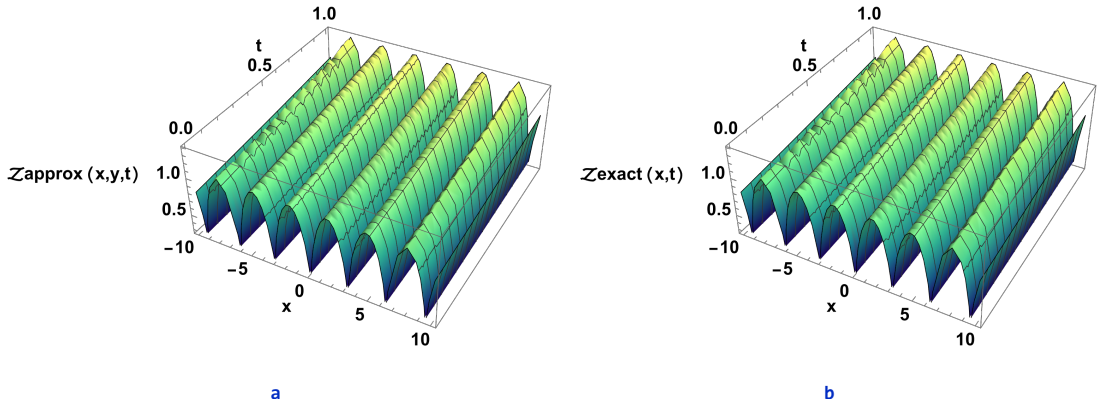

Figure 9. 3D depiction of the solution to the TFNBPM (Malthusian law case II) at $y = 1$. (a) The estimated solution from Eq (5.17) at $\mathcal{B} = 1$; (b) the exact solution.

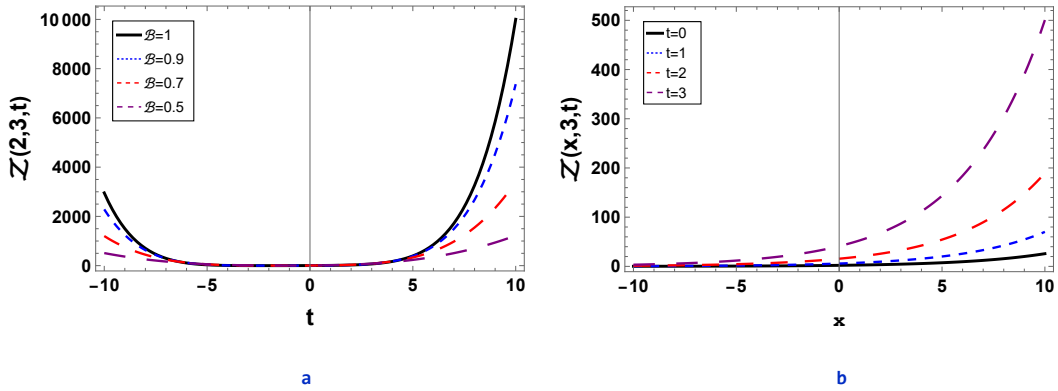

Figure 10. Two-dimensional solution profile of TFNBPM (Verhulst law for population) presented in Eq (5.30) at $r = 0.5$ and $\hbar = -1$. (a) For x = 2, and $y = 3$ at various $\mathcal{B}$ values; (b) for $y = 3$ and several time steps.

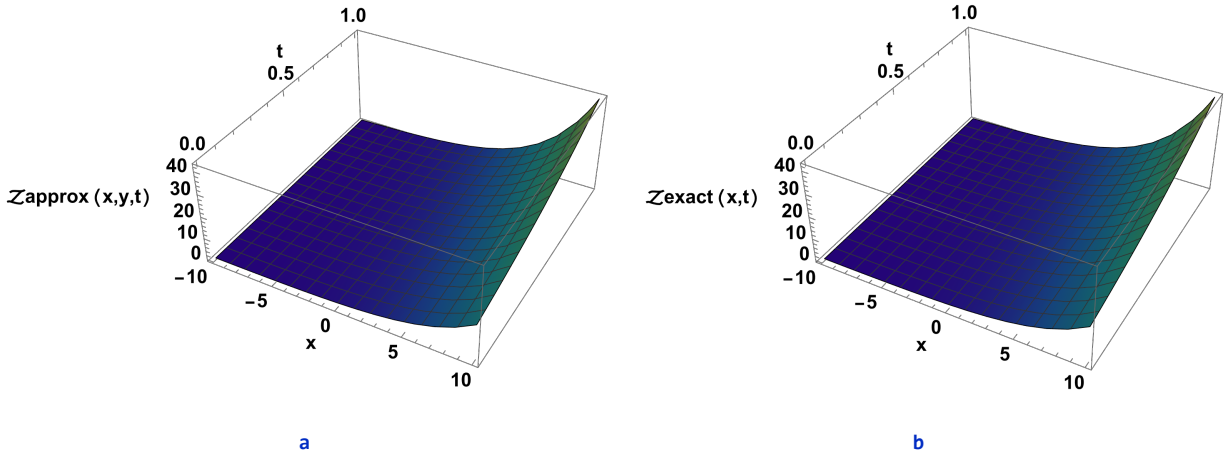

Figure 11. Three-dimensional profile of the solution of the TFNBPM (Verhulst law for population) at $y = 1$. (a) The approximated solution from Eq (5.30) at $\mathcal{B} = 1$; (b) the exact solution.

7. Conclusions

In this paper, we presented an in-depth analysis of the 2+1 nonlinear time-fractional generalized biological population model using the J-transform in conjunction with the optimal homotopy analysis method. The semi-analytical approach demonstrated its effectiveness in providing accurate and convergent solutions, which were validated through a series of 2D and 3D graphical representations. We presented two cases for the TFNBPM depending on the growth rate function called Malthusian and Verhulst low for population growth. Additionally, comparative studies with other established techniques underscored the robustness and efficiency of our proposed method. The findings of this research highlight the potential of combining the J-transform with optimal HAM to address complex fractional differential equations in biological population models.

Future research directions could focus on extending this approach to more complex and higher-dimensional fractional systems, exploring its application in other fields such as physics and engineering. Additionally, further refinement of the method to enhance computational efficiency and accuracy could be pursued. Investigating the integration of machine learning techniques with the J-transform and optimal HAM may also open new avenues for solving a broader range of nonlinear fractional differential equations.

Author contributions

Khalid K. Ali, Mohamed S. Mohamed and M. Maneea: Conceptualization, Methodology, Validation, Writing-original draft, Writing-review & editing. All authors of this article have been contributed equally. All authors have read and approved the final version of the manuscript for publication.

Funding

This research was funded by Taif University, Saudi Arabia, Project No. (TU-DSPP-2024-73).

Acknowledgments

The authors extend their appreciation to Taif University, Saudi Arabia, for supporting this work through project number (TU-DSPP-2024-73).

Conflict of interest

There is no conflict of interest between the authors or anyone else regarding this manuscript.

References

1. F. Shakeri, M. Dehghan, Numerical solution of a biological population model using He's variational iteration method, *Comput. Math. Appl.*, **54** (2007), 1197–1209. https://doi.org/10.1016/j.camwa.2006.12.076

2. M. Shakeel, M. Iqbal, S. Mohyud-Din, Closed form solutions for nonlinear biological population model, *J. Biol. Syst.*, **26** (2018), 207–223. https://doi.org/10.1142/S0218339018500109

3. M. Uddin, H. Ali, M. Taufiq, On the approximation of a nonlinear biological population model using localized radial basis function method, *Math. Comput. Appl.*, **24** (2019), 54. https://doi.org/10.3390/mca24020054

4. S. Mohyud-Din, A. Ali, B. Bin-Mohsin, On biological population model of fractional order, *Int. J. Biomath.*, **9** (2016), 1650070. https://doi.org/10.1142/S1793524516500704

5. Z. Fan, K. Ali, M. Maneea, M. Inc, S. Yao, Solution of time fractional Fitzhugh-Nagumo equation using semi analytical techniques, *Results Phys.*, **51** (2023), 106679. https://doi.org/10.1016/j.rinp.2023.106679

6. K. Ali, M. Maneea, Optical solitons using optimal homotopy analysis method for time-fractional (1+1)-dimensional coupled nonlinear Schrodinger equations, *Optik*, **283** (2023), 170907. https://doi.org/10.1016/j.ijleo.2023.170907

7. K. Ali, M. Maneea, M. Mohamed, Solving nonlinear fractional models in superconductivity using the q-Homotopy analysis transform method, *J. Math.*, **2023** (2023), 6647375. https://doi.org/10.1155/2023/6647375

8. S. Alsallami, M. Maneea, E. Khalil, S. Abdel-Khalek, K. Ali, Insights into time fractional dynamics in the Belousov-Zhabotinsky system through singular and non-singular kernels, *Sci. Rep.*, **13** (2023), 22347. https://doi.org/10.1038/s41598-023-49577-1

9. M. Du, Z. Wang, H. Hu, Measuring memory with the order of fractional derivative, *Sci. Rep.*, **3** (2013), 3431. https://doi.org/10.1038/srep03431

10. A. Ivanov, Fractional activation functions in feedforward artificial neural networks, *Proceedings of 20th International Symposium on Electrical Apparatus and Technologies (SIELA)*, 2018, 1–4. https://doi.org/10.1109/SIELA.2018.8447139

11. K. Ali, A. Wazwaz, M. Maneea, Efficient solutions for fractional Tsunami shallow-water mathematical model: a comparative study via semi analytical techniques, *Chaos Soliton. Fract.*, **178** (2024), 114347. https://doi.org/10.1016/j.chaos.2023.114347

12. K. Raslan, K. Ali, Numerical study of MHD-duct flow using the two-dimensional finite difference method, *Appl. Math. Inf. Sci.*, **14** (2020), 693–697. https://doi.org/10.18576/amis/140417

13. A. Ali, M. Asjad, M. Usman, M. Inc, Numerical solutions of a heat transfer for fractional maxwell fluid flow with water based clay nanoparticles; a finite difference approach, *Fractal Fract.*, **5** (2021), 242. https://doi.org/10.3390/fractalfract5040242

14. Z. Zhang, G. Li, Lie symmetry analysis and exact solutions of the time-fractional biological population model, *Physica A*, **540** (2020), 123134. https://doi.org/10.1016/j.physa.2019.123134

15. Z. Zhang, Z. Lin, Local symmetry structure and potential symmetries of time-fractional partial differential equations, *Stud. Appl. Math.*, **147** (2021), 363–389. https://doi.org/10.1111/sapm.12374

16. H. Zhu, Z. Zhang, J. Zheng, The time-fractional (2+1)-dimensional Hirota-Satsuma-Ito equations: Lie symmetries, power series solutions and conservation laws, *Commun. Nonlinear Sci.*, **115** (2022), 106724. https://doi.org/10.1016/j.cnsns.2022.106724

17. M. Akram, T. Ihsan, T. Allahviranloo, Solving Pythagorean fuzzy fractional differential equations using Laplace transform, *Granul. Comput.*, **8** (2023), 551–575. https://doi.org/10.1007/s41066-022-00344-z

18. S. Rashid, K. Kubra, K. Abualnaja, Fractional view of heat-like equations via the Elzaki transform in the settings of the Mittag-Leffler function, *Math. Method. Appl. Sci.*, **46** (2023), 11420–11441. https://doi.org/10.1002/mma.7793

19. K. Ali, M. Mohamed, M. Maneea, Exploring optical soliton solutions of the time fractional q-deformed Sinh-Gordon equation using a semi-analytic method, *AIMS Mathematics*, **8** (2023), 27947–27968. https://doi.org/10.3934/math.20231429

20. D. Albogami, D. Maturi, H. Alshehri, Adomian decomposition method for solving fractional Time-Klein-Gordon equations using Maple, *Applied Mathematics*, **14** (2023), 411–418. https://doi.org/10.4236/am.2023.146024

21. S. Maitama, W. Zhao, Beyond Sumudu transform and natural transform: J-transform properties and applications, *J. Appl. Anal. Comput.*, **10** (2020), 1223–1241. https://doi.org/10.11948/20180258

22. B. Singh, A. Kumar, M. Gupta, Efficient new approximations for space-time fractional multi-dimensional telegraph equation, *Int. J. Appl. Comput. Math.*, **8** (2022), 218. https://doi.org/10.1007/s40819-022-01343-z

23. B. Singh, A. Kumar, S. Rai, D. Prakasha, Study of nonlinear time-fractional hyperbolic-like equations with variable coefficients via semi-analytical technique: differential J-transform method, *Int. J. Mod. Phys. B*, **38** (2024), 2450001. https://doi.org/10.1142/S0217979224500012

24. V. Srivastava, S. Kumar, M. Awasthi, B. Singh, Two-dimensional time fractional-order biological population model and its analytical solution, *Egyptian Journal of Basic and Applied Sciences*, **1** (2014), 71–76. https://doi.org/10.1016/j.ejbas.2014.03.001

25. O. Acana, M. Al Qurashi, D. Baleanu, New exact solution of generalized biological population model, *J. Nonlinear Sci. Appl.*, **10** (2017), 3916–3929. https://doi.org/10.22436/jnsa.010.07.44

26. P. Veeresha, D. Prakasha, An efficient technique for two-dimensional fractional order biological population model, *Int. J. Model. Simul. Sci.*, **2020** (2020), 2050005. https://doi.org/10.1142/S1793962320500051

27. D. Ziane, M. Hamdi Cherif, D. Baleanu, K. Belghaba, Non-differentiable solution of nonlinear biological population model on cantor sets, *Fractal Fract.*, **4** (2020), 5. https://doi.org/10.3390/fractalfract4010005

28. M. Alaroud, A. Alomari, N. Tahat, A. Ishak, Analytical computational scheme for multivariate nonlinear time-fractional generalized biological population model, *Fractal Fract.*, **7** (2023), 176. https://doi.org/10.3390/fractalfract7020176

29. I. Podlubny, *Fractional differential equations: an introduction to fractional derivatives, fractional differential equations, to methods of their solution and some of their applications*, San Diego: Academic Press, 1999.

30. R. Khalil, M. Al Horani, A. Yousef, M. Sababheh, A new definition of fractional derivative, *J. Comput. Appl. Math.*, **264** (2014), 65–70. https://doi.org/10.1016/j.cam.2014.01.002

31. A. Elsaid, M. Latif, M. Maneea, Similarity solutions for solving Riesz fractional partial differential equations, *Progr. Fract. Differ. Appl.*, **2** (2016), 293–298. https://doi.org/10.18576/pfda/020407

32. S. Liao, *Beyond perturbation: introduction to the homotopy analysis method*, New York: Chapman and Hall/CRC, 2003. https://doi.org/10.1201/9780203491164

33. V. Marinca, N. Herisanu, Application of optimal homotopy asymptotic method for solving nonlinear equations arising in heat transfer, *Int. Commun. Heat Mass*, **35** (2008), 710–715. https://doi.org/10.1016/j.icheatmasstransfer.2008.02.010

34. S. Liao, An optimal homotopy-analysis approach for strongly nonlinear differential equations, *Commun. Nonlinear Sci.*, **15** (2010), 2003–2016. https://doi.org/10.1016/j.cnsns.2009.09.002

35. A. El-Ajou, O. Arqub, Z. Al Zhour, S. Momani, New results on fractional power series: theories and applications, *Entropy*, **15** (2013), 5305–5323. https://doi.org/10.3390/e15125305

36. Y. Liu, Z. Li, Y. Zhang, Homotopy perturbation method to fractional biological population equation, *Fractional Differential Calculus*, **1** (2011), 117–124. https://doi.org/10.7153/fdc-01-07

AIMS Press